

Article

An All-Fiber Curvature Sensor with High Sensitivity Based on Sphere-Shaped Misaligned Structure

Xiaowei Li, Qiangshen Chen, Mengyu Ren and Guoying Feng * 

Institute of Laser & Micro/Nano Engineering, College of Electronics and Information Engineering, Sichuan University, Chengdu 610064, China; lixiaowei@stu.scu.edu.cn (X.L.); 2022322055035@scu.stu.edu.cn (Q.C.); renmengyu@stu.scu.edu.cn (M.R.)

* Correspondence: guoying_feng@scu.edu.cn

Abstract: In this paper, a high-linear-sensitivity fiber curvature sensor based on the sphere-shaped misaligned structure (SSMS) with few-mode fiber (FMF) and single-mode fiber (SMF) was proposed and demonstrated. A spherical structure was prepared at one end of a few-mode fiber, which could effectively excite higher-order modes and generate interference in the misaligned cascade. When external environmental parameters changed, the resonance peaks formed by intermodal interference were displaced, and the shifts generated by different resonant peaks were also different. The experimental results show that the maximum curvature sensitivity was -2.220 nm/m^{-1} , and the linear fitting coefficient reached up to 0.991, which is an extremely high sensitivity among wavelength-modulated curvature sensors. Meanwhile, the strain sensitivity of the sensor was as low as $7.99 \text{ pm}/\mu\bar{\epsilon}$, and the temperature sensitivity was $3.958 \text{ pm}/^{\circ}\text{C}$, which is a low temperature sensitivity and low strain sensitivity, and solves the cross-sensitivity problem. With advantages of simple manufacture, low cost, and favorable stability, the sensor is expected to be one of the best candidate instruments for measuring curvature and inclination.

Keywords: few-mode fiber; Mach–Zehnder interference; curvature sensing; strain; temperature



Academic Editors: Jose Rafael Guzman-Sepulveda and Arturo Alberto Castillo-Guzmán

Received: 7 November 2024

Revised: 26 December 2024

Accepted: 14 January 2025

Published: 17 January 2025

Citation: Li, X.; Chen, Q.; Ren, M.; Feng, G. An All-Fiber Curvature Sensor with High Sensitivity Based on Sphere-Shaped Misaligned Structure. *Optics* **2025**, *6*, 3. <https://doi.org/10.3390/opt6010003>

Copyright: © 2025 by the authors. Licensee MDPI, Basel, Switzerland. This article is an open access article distributed under the terms and conditions of the Creative Commons Attribution (CC BY) license (<https://creativecommons.org/licenses/by/4.0/>).

1. Introduction

Sensing technology is widely used in environmental monitoring, healthcare, safety monitoring, intelligent transportation, agricultural production, and other fields. Compared to other sensors [1–5], optical fiber sensors (FOSs) [6–9] based on optical fiber sensing technology have attracted more and more attention due to their unique anti-electromagnetic interference, compactness, high sensitivity, and corrosion resistance. Optical fiber sensors can be used to monitor various physical variables in the external environment, including temperature [10], strain [11,12], refractive index (RI) [13–16], magnetic field [17], humidity [18,19], curvature [20–22], pH [23], displacement [24,25], shape [26–29], and so on [30].

Among them, optical fiber curvature sensing technology is one of the important application directions of FOSs. In recent years, a great deal of work has been carried out in preparing novel fiber optic sensor structures. In 2020, Tan et al. [19] proposed a temperature and vector curvature sensor based on dual-core photonic crystal fiber, which is capable of achieving $61.68 \text{ pm}/^{\circ}\text{C}$ temperature sensing and bidirectional curvature sensing. In 2021, Wang et al. [31] introduced a curvature and temperature sensor with a tapered dispersion compensation fiber; the curvature sensitivity and a temperature sensitivity were 15.19 dB/m^{-1} and $79.8 \text{ pm}/^{\circ}\text{C}$, respectively. In 2023, Escobar-Vera et al. [22] presented a system by interrogating three cores of a multicore fiber (MCF) with the time-expanded

phase-sensitive (TE- Φ) OTDR technique, which was able to perform distributed curvature sensing over a range of 125 m, with a resolution of 10 cm, and a sampling rate of 50 Hz. In 2024, Wu et al. [32] made a curvature fiber sensor that achieved a maximum curvature sensitivity of -96.70 dB/m^{-1} and a temperature sensitivity of $212 \text{ pm}/^\circ\text{C}$. The sensitivity and measuring range of the above sensors are limited, and the high temperature cross-sensitivity greatly affects the accuracy of curvature detection and limits the accurate measurement of curvature sensing. Unfortunately, the aforementioned curvature sensors are usually subject to external environmental parameters, which reduces the accuracy of curvature sensing.

In this paper, a hybrid sphere-shaped misaligned structure curvature sensor based on the SMF-FMF-SMF (SFS-SSMS) is proposed. The sensor is fabricated by splicing a section of FMF between two SMFs with a spherical microstructure and a misaligned structure, and the simple structure effectively increases the range of the curvature measurement. Experimental results show that the curvature sensor achieved a high curvature sensitivity of -2.220 nm/m^{-1} , with a low axial strain response and low temperature response, which can effectively solve the problem of cross-sensitivity. In addition, the proposed fiber curvature sensor has the advantages of good mechanical properties, easy use, and repeatable and reversible sensing response, improving the practicability and flexibility of the sensor in engineering.

2. Materials and Methods

The manufacturing process of the sensor is simple and repeatable. First, the relevant parameters of the fiber splicing program in the splicing machine (Signal Fire X, Signal Fire Technology Co., Ltd., Chengdu, China) are as follows: dust removal voltage 120 mV, dust removal time 200 ms and 150 ms; fiber pre-melting voltage 10 mV, pre-melting time 180 ms; welding voltage 940 mV, and welding time 3000 ms. Under the above parameters, the fusion splicer performs multiple discharges on the FMF (YOFC FM SI-4, Yangtze Optical Fibre and Cable Joint Stock Limited Company, Wuhan, China) fiber end face. During the arc discharge process, the left stepping motor is pushed to the right, which causes the softened portion of the fiber to be squeezed and gradually expand into a spherical structure. After that, one end of the FMF with a spherical structure is axially fused to a single-mode fiber, while the other plane of the FMF is misaligned with another SMF (Corning SMF28e, Corning Incorporated, Shanghai, China). The sensing structure can be stably and reproducibly prepared, and the preparation process is simple and environmentally friendly, as shown in Figure 1.

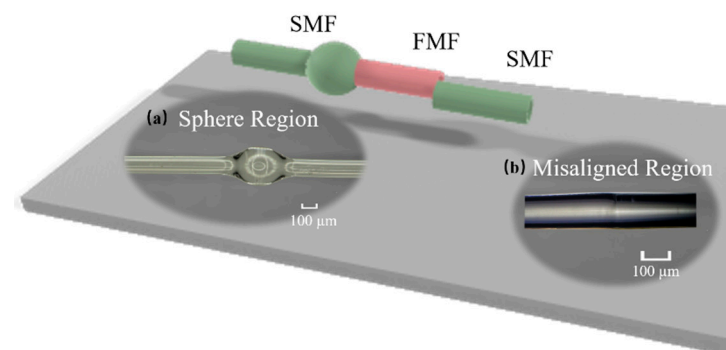


Figure 1. Structure diagram of the SFS-SSMS structure sensor. (a) Micrograph of the sphere region. (b) Micrograph of the misaligned region.

When light reaches the fusion region of SMF and FMF, the high-order modes are excited due to the spherical microstructure, and the specially designed structure of the fusion region will enhance the interference effect and improve the curvature sensitivity. The high-order modes transmit along the FMF, and interference occurs when reaching the misalignment region between the FMF and SMF on the right side of the structure. Hence, this FMF microstructure interferometer can be considered as an MZI.

Based on the above analysis, the wavelength changes of the interference trough of MZI based on FMF can be given by

$$\Delta\lambda = \frac{\lambda_m^2}{\Delta n_{\text{eff}} L} \frac{\Delta\varphi}{2\pi} \quad (1)$$

where $\Delta n_{\text{eff}} = n_{\text{eff}}^{\text{co}} - n_{\text{eff}}^{\text{cl}}$, $n_{\text{eff}}^{\text{co}}$, and $n_{\text{eff}}^{\text{cl}}$ are the effective RIs of the core mode and the cladding mode, respectively; L is the distance between two excitation/coupling units, which is the distance between the spherical structure and the misaligned structure; and λ_m is the wavelength of the interference trough.

When the temperature is constant, any change in the curvature of the sensing structure will affect the wavelength of the interference trough. Assuming that the structural length variation is ΔL , then $\Delta L = \gamma\Delta C$, where γ represents the correlation coefficient between the curvature change and the structure length, and ΔC is the curvature change. The phase difference of the sensor can be expressed as

$$\Delta\varphi = \frac{2\pi}{\lambda_m} \left[\Delta n_{\text{eff}} \gamma \Delta C + (p_e^{\text{co}} n_{\text{eff}}^{\text{co}} \gamma \Delta C - p_e^{\text{cl}} n_{\text{eff}}^{\text{cl}} \gamma \Delta C) L \right] \quad (2)$$

where p_e^{co} and p_e^{cl} are the effective elastic coefficients of the core and the cladding. Therefore, the curvature sensing sensitivity of the sensor can be expressed as

$$\Delta\lambda = \lambda_m \gamma \left[\frac{1}{L} + \frac{(p_e^{\text{co}} n_{\text{eff}}^{\text{co}} \gamma - p_e^{\text{cl}} n_{\text{eff}}^{\text{cl}} \gamma)}{\Delta n_{\text{eff}}} \right] \Delta C \quad (3)$$

The light field properties of the sensor were simulated with the beam propagation method (BPM) module in RSoft software (Version 8.0.2.1), analyzing the mode excitation and inter-mode interference of the SFS-SSMS sensor. In the experiment, the diameters of the core and cladding of the SMF were 9 μm and 125 μm , respectively, and the corresponding refractive indices were 1.45 and 1.47, respectively. The diameters of the core and cladding of the FMF were 18.5 μm and 125 μm , respectively. The diameter of the spherical structure was 247 μm , and the misaligned distance was half the core size, about 9 μm .

Figure 2 shows the simulation results of the normalized transmission light field along the Mach-Zehnder Interferometer (MZI) at an input wavelength of 1064 nm. When the transmitted light passes through the spherical structure, the cladding high-order modes are excited, and then the light will be transmitted over a certain distance between the core and the cladding before being re-coupled into the core through the misaligned structure. Due to the phase difference between the core and cladding modes, interference occurs. From the simulation results, it can be found that between the spherical structure and the misaligned structure, the energy exchange occurs between the LP_{01} , LP_{02} , LP_{03} , LP_{04} , and LP_{21} modes, and the interference phenomenon is mainly generated by the LP_{01} and LP_{03} modes.

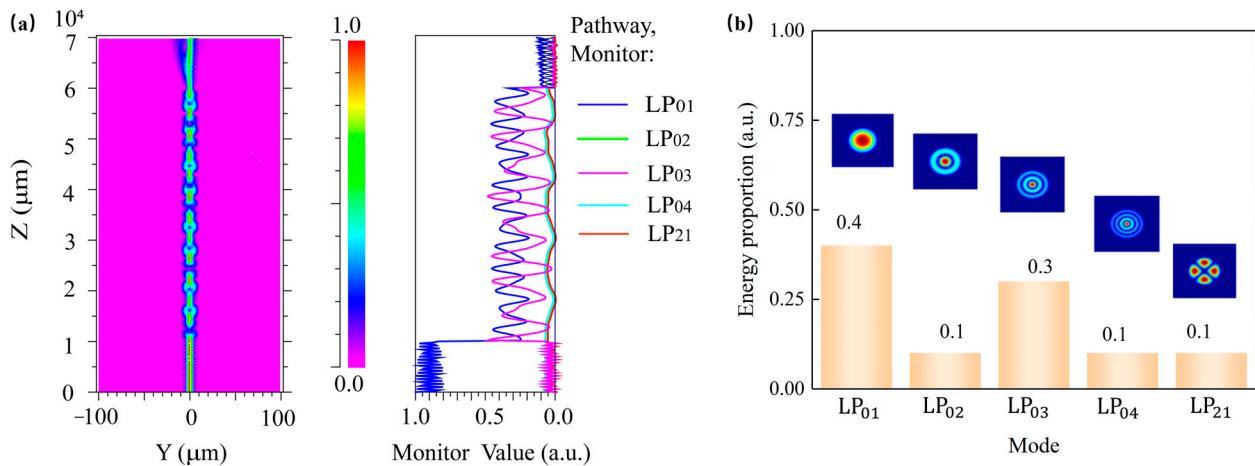


Figure 2. (a) Light field distribution and normalized energy distribution of the Mach–Zehnder Interferometer (MZI) at 1064 nm. (b) The energy proportion of different modes and the corresponding mode distribution.

3. Results and Discussion

Compared to other similar fiber sensors [33–36], the proposed fiber optic curvature sensor has higher responsiveness and lower strain and temperature sensitivity. It is insensitive to both strain and ambient temperature, thereby effectively avoiding the influence of other environmental parameters on curvature sensing in practical applications. The detailed analysis of the experimental results is as follows, as shown in Table 1.

Table 1. A comparison of the sensitivity of different sensors.

Structure	Refs.	Curvature	Strain	Temperature
SFS-SSMS	Our work	-2.220 nm/m^{-1}	$7.99 \text{ pm}/\mu\epsilon$	$3.958 \text{ pm}/^\circ\text{C}$
SCMCF	[33]	15.9 dB/m^{-1}	-	$-0.0179 \text{ dB}/^\circ\text{C}$
RCF-TAPER-SMF	[34]	-3.504 nm/m^{-1}	$0.292 \text{ pm}/\mu\epsilon$	$59.42 \text{ pm}/^\circ\text{C}$
ARRG-MZI	[35]	-2.02 nm/m^{-1}	-	$5.54 \text{ pm}/^\circ\text{C}$
UV-FBG	[36]	0.553 nm/m^{-1}	-	$20.57 \text{ pm}/^\circ\text{C}$

SFS-SSMS (SMF-FMF-SMF Sphere-Shaped Misaligned Structure); SCMCF (Strongly Coupled Multicore Fiber); RCF-TAPER-SMF (Ring Core Fiber); ARRG-MZI (Anti-Resonant Reflecting Guidance); UV-FBG (Fiber Bragg Grating).

In order to verify the theoretical analysis and simulation results, sensor curvature, strain, and temperature sensing were carried out in an ultra-clean optical laboratory with constant temperature (20 °C) and controlled humidity. The experimental setups are shown in Figure 3. Light was emitted from the broadband light source (Broadband Source, ASE-1064, Sichuan Zi Guan photonics technology Co., Ltd., Mianyang, China); the effective wavelength ranged from 1040 nm to 1160 nm) to the sensor via a fiber optic cable (SMF 28e, Shenzhen SDG Information Co., Ltd., Shenzhen, China), and the external variables were subsequently applied to the sensor. The transmission spectrum of the modulated signals was obtained by a spectrum analyzer (Optical Spectral Analyzer, YOKOGAWA AQ6370D, Yokogawa Test & Measurement (Shanghai) Co., Ltd., Shanghai, China), which has a maximum resolution of 0.02 nm.

The transmission spectrum of the light source (ASE-1064) at room temperature (20 °C) and the transmission spectrum of the sensor in the initial state (0 mm^{-1} , $0 \mu\epsilon$, 20 °C) are shown in Figure 4. The light purple curve shows the modulation spectrum of the SFS-SMMS structure sensor with obvious peaks and troughs. The light blue curve indicates the spectrum of the light source.

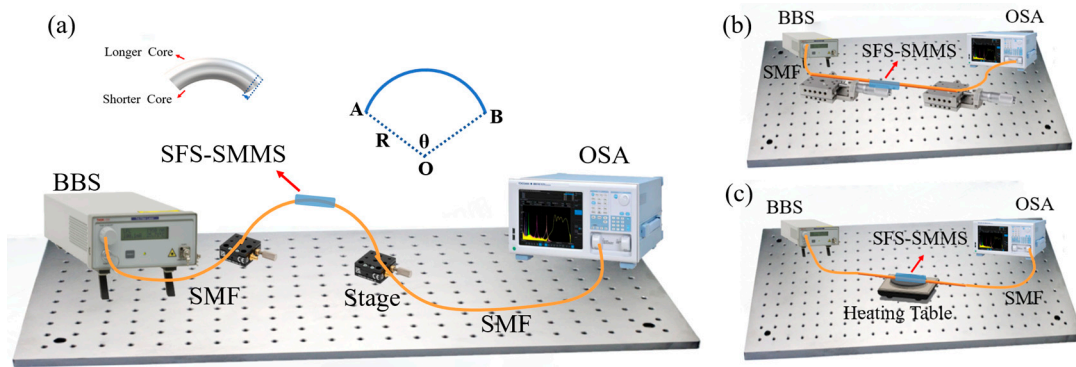


Figure 3. Experimental setups of the sensor. (a) Curvature; (b) axial strain; and (c) temperature. BBS—broadband source; OSA—optical spectral analyzer; SMF—single-mode fiber.

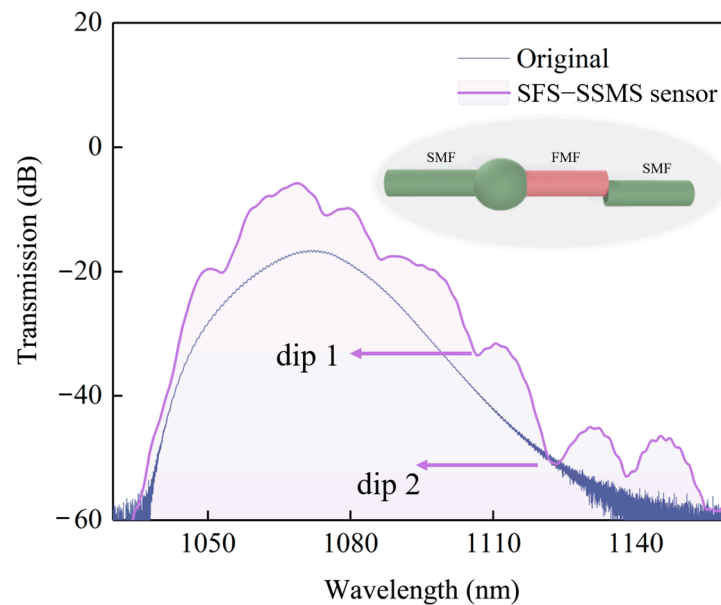


Figure 4. Transmission spectra of the light source and SFS-SSMS sensors.

Subsequently, the curvature sensing performance of the SFS-SSMS sensor was experimentally verified. The experimental sensing device is shown in Figure 3a. The structure was fixed on an elastic plastic plate, and the two ends of the plate were fixed on two collinear platforms. In the initial state, the plastic plate and the optical fiber sensing structure were kept straight, and the distance between the two platforms was 100 mm. Then, one side of the control platform was moved inward, causing the optical fiber and plastic plate to curve together. As the two displacement platforms moved alternately in a step of 0.5 mm, the elastic plastic plate was subjected to a uniform force, forming a standard arc as much as possible, and the spectrum was recorded. In Figure 3a, \overline{AB} is defined as the length of the arc, the length of the string is defined as AB , and the central angle is defined as θ . The arc radius R can be calculated by the arc length \overline{AB} and the chord length AB , and the curvature is $1/R, C = \frac{1}{R} = \sqrt{\frac{24d}{L^3}}$ [34,37]. The unit step change of the stage was 0.5 mm ($d = 0.5$ mm), the corresponding unit curvature change was $6.57 \times 10^{-4} \text{ mm}^{-1}$ ($\Delta C = 6.57 \times 10^{-4} \text{ mm}^{-1}$), and the total displacement of the stage was 6 mm.

In order to visualize the changes in the interference spectrum, we normalized the interference spectra. As can be seen in the insets of Figure 5a,b, the spectrum undergoes a significant blue shift as the curvature increases. The interferometric troughs close to 1088 nm (Dip 1) and 1103 nm (Dip 2) were chosen as the indicating troughs for curvature sensing. As the curvature increases, the wavelength position of the indicating troughs

(Dip 1, Dip 2) changes, with the linear fit coefficients reaching 0.991 (Dip 1) and 0.966 (Dip 2), respectively. The curvature sensitivities of the indicating troughs (Dip 1 and Dip 2) are about -2.220 nm/m^{-1} and -1.373 nm/m^{-1} , respectively. The negative sign only indicates that the indicator trough moved towards the short wavelength.

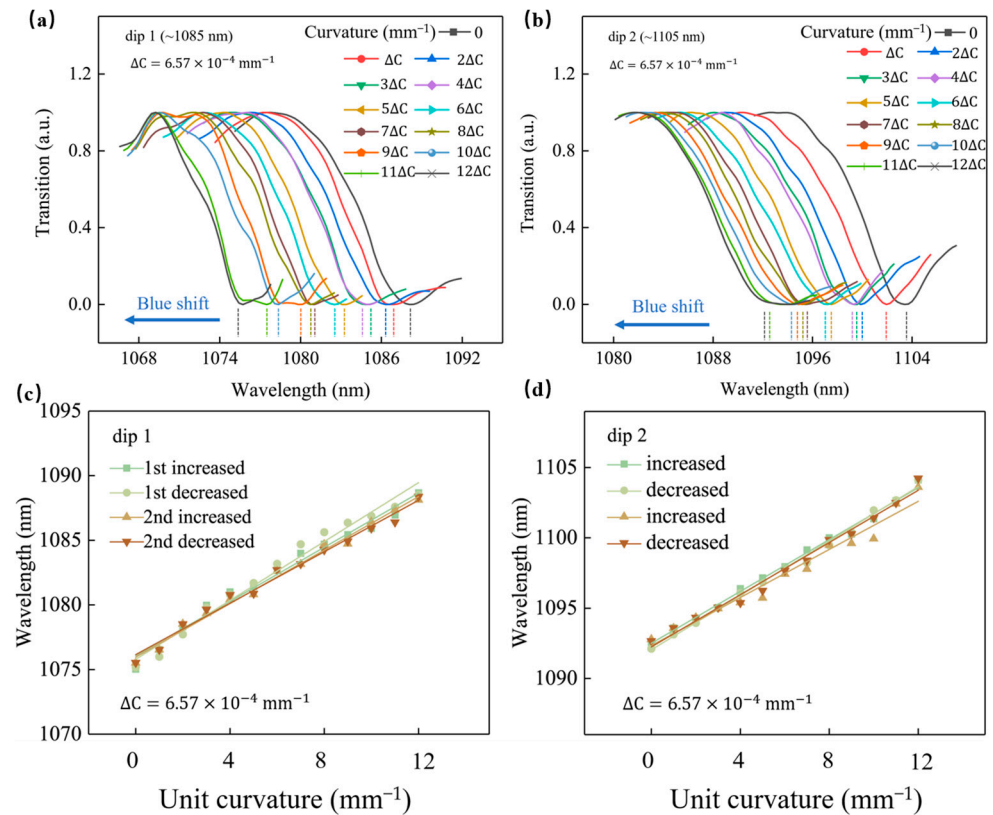


Figure 5. Interference spectral response of the sensor utilized in curvature sensing. (a) The interference trough near 1088 nm (Dip 1). (b) The interference trough near 1103 nm (Dip 2). Linear fitting curve of the indicating trough varying with curvature for (c) Dip 1 and (d) Dip 2.

In order to explore whether the sensor has directional (vector) bending characteristics, we conducted a reverse curvature sensing experiment, and selected Dip 1 (1088 nm, with the forward curvature sensitivity of -2.220 nm/m^{-1}) for analysis. The experimental results are shown in Figure 6. The spectrum undergoes a significant blue shift as the curvature increases. As the curvature increases, the wavelength position of Dip 1 changes, and the reverse curvature sensitivity of the Dip 1 is about -0.852 nm/m^{-1} , with the linear fit coefficients reaching 0.986.

Combined with the experimental results, the forward bending and reverse bending curvature sensitivities are -2.220 nm/m^{-1} (Dip 1) and -0.852 nm/m^{-1} , respectively. Unfortunately, the sensor cannot determine the direction of bending. The reason may be that the microstructure of the sensor is a symmetrical spherical structure with a misaligned cascade, with the misaligned distance of the structure is very small, and the whole structure is equal to symmetrical.

In order to explore the cross-sensitivity of the fiber structure to other environmental parameters, experiments on axial strain sensing and temperature sensing were also carried out. The sensing devices are shown in Figure 3b,c. The indicator trough, Dip 1 (~wavelength of 1088 nm), which has the highest curvature response sensitivity, was used to characterize the cross-response of the above environmental parameters. A linear fit was performed for the wavelength position of Dip 1 per unit environmental parameter ($\Delta\varepsilon$, ΔT , ΔC), and the results are shown in Figure 7.

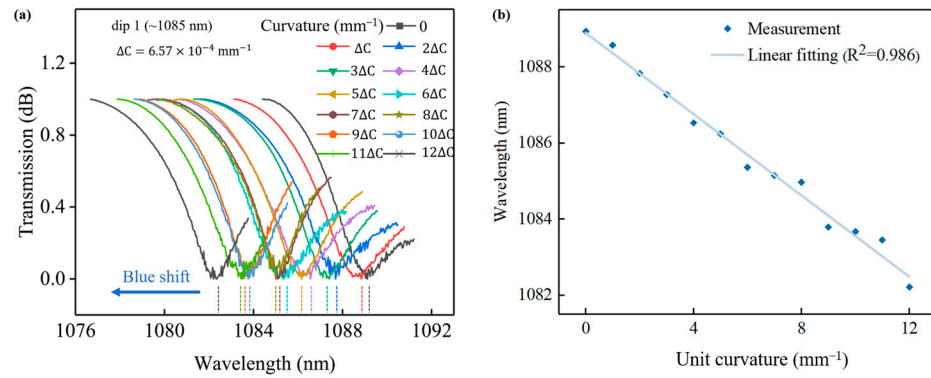


Figure 6. Interference spectral response of the sensor utilized in reverse curvature sensing. (a) The interference trough near 1088 nm (Dip 1). (b) Linear fitting curve of the indicating trough varying with curvature for Dip 1.

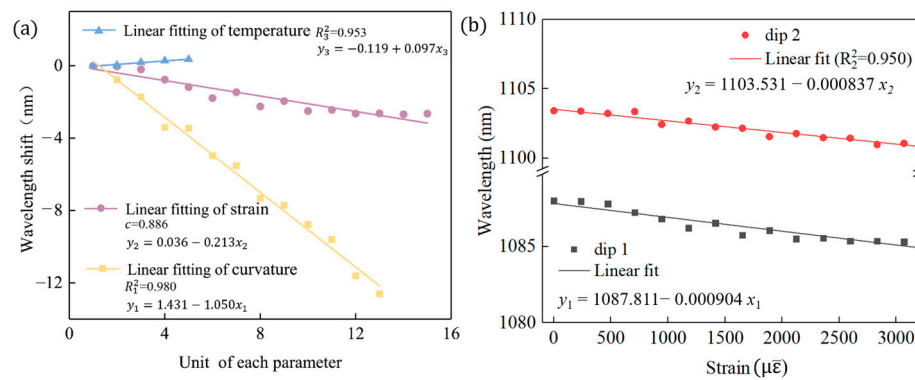


Figure 7. (a) Correspondence of wavelength movement of the indicating trough (Dip 1, 1088 nm) under unit changes of different environmental parameters. The blue curve is the temperature, the purple curve is the axial strain, and the yellow curve is the curvature. (b) Linear fitting curve of the indicating trough varying with strain for Dip 1 and Dip 2.

The cross-sensing experiments were divided into axial strain and temperature. The axial strain experimental process is outlined as follows: The two ends of the optical fiber were fixed on two collinear platforms. The distance between the two platforms was changed by controlling the micrometer knob on the right-hand translation platform, and the axial strain was applied to the optical fiber. The resolution of the micrometer was 0.001 mm. Let ϵ be the axial strain applied to the fiber; then, $\epsilon = \Delta l/L$, where Δl represents the length for each movement of the micrometer, and L is the initial distance between the two platforms ($L = 212$ mm). The unit step change of the translation stage was 0.005 mm, the corresponding unit strain was 2.36×10^{-5} ($\Delta\mu\epsilon = 23.6$), and the total displacement of the translation stage was 0.07 mm, with the corresponding total strain of 3.304×10^{-4} . For temperature sensing, the sensor was placed horizontally on a heating platform and covered with a quartz boat. The temperature range was 20–140 °C, with a heating interval of 30 °C ($\Delta T = 30$ °C). After the preset sampling temperature was reached, the transmission spectrum was recorded.

The purple line shows the linear fitting result of the indicating trough (Dip 1) under different strain conditions. In the strain range of 0–330.4 $\mu\epsilon$, the indicating trough (Dip 1) gradually blue-shifts as the applied axial strain increases. It can be seen that the maximum strain sensitivity was about 7.99 pm/ $\mu\epsilon$. The sensor exhibited a very low strain sensitivity across a wide strain range, indicating that the proposed sensor is essentially strain-insensitive.

As shown in blue, the wavelength shift range of the indicating trough (Dip 1) is less than 0.5 nm across the entire temperature range (20 °C to 140 °C, with a unit temperature

interval of 30 °C; $\Delta T = 30$ °C). The temperature sensitivity was very low at 2.958 pm/°C, which can be considered negligible for curvature sensing.

When the sensor is measuring a certain environmental parameter, the phenomenon of cross-response usually occurs. The experiment was carried out in an optical laboratory with constant temperature and humidity, and the temperature had little effect on the sensor, so we used the two-wavelength matrix method to analyze the curvature and strain.

The wavelength shifts of the indicated trough (Dip 1, Dip 2) caused by external environmental curvature, strain, and temperature changes can be expressed as follows [38]:

$$\Delta\lambda_i = K_{C_i}\Delta C + K_{\varepsilon_i}\Delta\varepsilon \quad (4)$$

where K_{C_i} and K_{ε_i} are the strain sensitivity and temperature sensitivity. The strain sensitivities of the indicating troughs are -0.000904 nm/ $\mu\bar{\varepsilon}$ and -0.00837 nm/ $\mu\bar{\varepsilon}$, respectively. The response relationship with the change in environmental parameters is linear. Therefore, Equation (4) can be rewritten as a matrix:

$$\begin{bmatrix} \Delta C \\ \Delta\varepsilon \end{bmatrix} = \begin{bmatrix} K_{C1} & K_{\varepsilon1} \\ K_{C2} & K_{\varepsilon2} \end{bmatrix} \begin{bmatrix} \Delta\lambda_1 \\ \Delta\lambda_2 \end{bmatrix} \quad (5)$$

Bringing the above experimental results into a matrix, Equation (5) can be rewritten as follows:

$$\begin{bmatrix} \Delta C \\ \Delta\varepsilon \end{bmatrix} = \begin{bmatrix} -2.220 & -0.000904 \\ -1.373 & -0.000837 \end{bmatrix} \begin{bmatrix} \Delta\lambda_1 \\ \Delta\lambda_2 \end{bmatrix} \quad (6)$$

4. Conclusions

In summary, we designed and experimentally proved an MZI-based SSMS-SFS hybrid all-fiber curvature sensor. The sensor was prepared by simple arc discharge fusion of cascaded spherical misaligned microstructures by SMF and FMF. In terms of curvature measurement, the sensor achieved a peak curvature sensitivity of -2.220 nm/m⁻¹. Meanwhile, the sensor also demonstrated low strain and temperature sensitivity. When the strain varied from 0 to 330.4 $\mu\bar{\varepsilon}$, the highest strain sensitivity was 7.99 pm/ $\mu\bar{\varepsilon}$, and the highest temperature sensitivity was 3.958 pm/°C when the temperature changed from 20 °C to 140 °C. In addition, the sensor's curvature sensing repeatability is excellent, and the sensing sensitivity is linear over the entire measurement range. Since the sensor has the advantages of low cost, simple preparation, and compact structure, it can be effectively applied to curvature sensing in small spaces, and it can also be easily multiplexed into fiber optic sensor networks, offering very broad application prospects in structural health monitoring, robotics, biomedical engineering, and other industries. Furthermore, it provides new possibilities for curvature sensing research and applications.

Author Contributions: X.L.: methodology, software, investigation, formal analysis, writing—original draft. Q.C.: conceptualization, data curation, writing—original draft. M.R.: writing—review and editing. G.F.: conceptualization, funding acquisition, resources, supervision, writing—review and editing. All authors have read and agreed to the published version of the manuscript.

Funding: This research was supported by international science and technology cooperation projects funded by the Chengdu Municipal Government (No. 2022-GH02-00017-HZ) and the international cooperation projects of Sichuan Province (No. 2023YFH0094).

Data Availability Statement: Dataset available on request from the authors. The raw data supporting the conclusions of this article will be made available by the authors on request.

Conflicts of Interest: The authors declare that they have no known competing financial interests or personal relationships that could have appeared to influence the work reported in this paper.

References

1. Chang, S.M.; Muramatsu, H.; Nakamura, C.; Miyake, J. The principle and applications of piezoelectric crystal sensors. *Mater. Sci. Eng. C* **2000**, *12*, 111–123. [[CrossRef](#)]
2. Zhou, Q.; Lam, K.H.; Zheng, H.; Qiu, W.; Shung, K.K. Piezoelectric single crystal ultrasonic transducers for biomedical applications. *Prog. Mater. Sci.* **2014**, *66*, 87–111. [[CrossRef](#)]
3. Quintana-Diaz, G.; Mena-Rodriguez, P.; Perez-Alvarez, I.; Jimenez, E.; Dorta-Naranjo, B.-P.; Zazo, S.; Perez, M.; Quevedo, E.; Cardona, L.; Joaquin Hernandez, J. Underwater electromagnetic sensor networks-part I: Link characterization. *Sensors* **2017**, *17*, 189. [[CrossRef](#)]
4. Chen, D.; Li, Y.; Pan, M.; Tian, W. Flexible planar electromagnetic sensor array fabricated with printing electronic technology. *Measurement* **2018**, *129*, 499–503. [[CrossRef](#)]
5. Fiorillo, A.S.; Critello, C.D.; Pullano, S.A. Theory, technology and applications of piezoresistive sensors: A review. *Sens. Actuators A Phys.* **2018**, *281*, 156–175. [[CrossRef](#)]
6. Leal-Junior, A.G.; Marques, C. Diaphragm-embedded optical fiber sensors: A review and tutorial. *IEEE Sens. J.* **2021**, *21*, 12719–12733. [[CrossRef](#)]
7. Liu, Z.; Tam, H.-Y.; Lin, H.; Tse, M.-L.V.; Lu, C. Microstructured optical fiber sensors. *J. Light. Technol.* **2017**, *35*, 3425–3439. [[CrossRef](#)]
8. Zhao, Y.; Shen, J.; Liu, Q.; Zhu, C. Optical fiber sensor based on helical fibers: A review. *Measurement* **2022**, *188*, 110400. [[CrossRef](#)]
9. Wang, J.; Han, Y.; Cao, Z.; Xu, X.; Zhang, J.; Xiao, F. Applications of optical fiber sensor in pavement Engineering: A review. *Constr. Build. Mater.* **2023**, *400*, 132713. [[CrossRef](#)]
10. Militky, J.; Kadulova, M.; Ciprian, D.; Hlubina, P. Fiber optic temperature sensing with enhanced sensitivity based on spectral interferometry. *Opt. Fiber Technol.* **2017**, *33*, 45–50. [[CrossRef](#)]
11. Tripathi, S.M.; Kumar, A.; Varshney, R.K.; Kumar, Y.B.P.; Marin, E.; Meunier, J.P. Strain and temperature sensing characteristics of single-mode-multimode-single-mode structures. *J. Light. Technol.* **2009**, *27*, 2348–2356. [[CrossRef](#)]
12. Liu, C.; Guo, C.; Shao, Y.; Wei, Y.; Zhang, Z.; Ren, P.; Liu, C.; Shi, C.; Tang, Y.; Liu, Z. High sensitivity strain and refractive index MZI-SPR sensing based on dual fiber winding structure. *Opt. Express* **2024**, *32*, 24293–24303. [[CrossRef](#)]
13. Mukherjee, A.; Munsri, D.; Saxena, V.; Rajput, R.; Tewari, P.; Singh, V.; Ghosh, A.K.; John, J.; Wanare, H.; Gupta-Bhaya, P. Characterization of a fiber optic liquid refractive index sensor. *Sens. Actuators B Chem.* **2010**, *145*, 265–271. [[CrossRef](#)]
14. Wang, X.; Zhao, C.; Wang, Y.; Jin, S. A proposal of T-structure fiber-optic refractive index sensor based on surface plasmon resonance. *Opt. Commun.* **2016**, *369*, 189–193. [[CrossRef](#)]
15. Fu, X.; Zhou, J.; Fu, Z.; Xu, M.; Huang, S.; Jin, W.; Fu, G.; Bi, W. A multiparameter sensor based on dumbbell-shaped double-cladding fiber structure cascaded long period fiber grating. *IEEE Sens. J.* **2022**, *22*, 14118–14127. [[CrossRef](#)]
16. Wang, J.; Lu, X.; Mi, C.; Yin, Q.; Lv, J.; Yang, L.; Liu, W.; Yi, Z.; Liu, Q.; Chu, P.K.; et al. Ultra-high sensitivity photonic crystal fiber sensor based on dispersion turning point sensitization of surface plasmonic polariton modes for low RI liquid detection. *Opt. Express* **2024**, *32*, 32895–32908. [[CrossRef](#)] [[PubMed](#)]
17. Luo, L.; Pu, S.; Dong, S.; Tang, J. Fiber-optic magnetic field sensor using magnetic fluid as the cladding. *Sens. Actuators A Phys.* **2015**, *236*, 67–72. [[CrossRef](#)]
18. Xia, L.; Li, L.; Li, W.; Kou, T.; Liu, D. Novel optical fiber humidity sensor based on a no-core fiber structure. *Sens. Actuators A Phys.* **2013**, *190*, 1–5. [[CrossRef](#)]
19. Gu, B.; Yin, M.; Zhang, A.P.; Qian, J.; He, S. Optical fiber relative humidity sensor based on FBG incorporated thin-core fiber modal interferometer. *Opt. Express* **2011**, *19*, 4140–4146. [[CrossRef](#)]
20. Song, H.; Gong, H.; Ni, K.; Dong, X. All fiber curvature sensor based on modal interferometer with waist enlarge splicing. *Sens. Actuators A Phys.* **2013**, *203*, 103–106. [[CrossRef](#)]
21. Gong, Y.; Zhao, T.; Rao, Y.; Wu, Y. All-fiber curvature sensor based on ulmtimode interference. *IEEE Photonics Technol. Lett.* **2011**, *23*, 679–681. [[CrossRef](#)]
22. Escobar-Vera, C.; Soriano-Amat, M.; Martins, H.F.; Barrera, D.; Martin-Lopez, S.; Gonzalez-Herraez, M.; Fernández-Ruiz, M.R. Dynamic curvature sensing using time expanded Φ OTDR. *Opt. Lett.* **2023**, *48*, 4336–4339. [[CrossRef](#)] [[PubMed](#)]
23. Zhang, Z.; Yin, Z.; Li, S.; Hu, L. Cascaded dual-parameter SPR fiber sensor for RI and pH simultaneous detection based on Ag film and an Ag/self-assembled nanofilm structure. *Opt. Express* **2024**, *32*, 33330–33343. [[CrossRef](#)]
24. Mehta, A.; Mohammed, W.; Johnson, E.G. Multimode interference-based fiber-optic displacement sensor. *IEEE Photonics Technol. Lett.* **2003**, *15*, 1129–1131. [[CrossRef](#)]
25. Wei, Y.; Shi, C.; Liu, C.; Liu, C.; Wang, X.; Tang, Y.; Wang, R.; Liu, Z. Three-dimensional micro displacement sensor based on fiber SPR mechanisms. *Opt. Express* **2023**, *31*, 6411–6425. [[CrossRef](#)]

26. Tian, Y.; Dang, H.; Liu, W.; Cui, J.; Li, Y.; Tan, J. Structure shape measurement method based on an optical fiber shape sensor. *Meas. Sci. Technol.* **2023**, *34*, 85102. [[CrossRef](#)]
27. Fu, C.; Meng, Y.; Chen, L.; Zhong, H.; Du, C.; He, J.; Weng, X.; Liu, L.; Qu, J.; Wang, Y. High-spatial-resolution φ -OFDR shape sensor based on multicore optical fiber with femtosecond-laser-induced permanent scatter arrays. *Opt. Lett.* **2023**, *48*, 3219–3222. [[CrossRef](#)]
28. Wu, H.; Liang, L.; Wang, H.; Dai, S.; Xu, Q.; Dong, R. Design and Measurement of a Dual FBG High-Precision Shape Sensor for Wing Shape Reconstruction. *Sensors* **2021**, *22*, 168. [[CrossRef](#)]
29. Fu, C.; Xiao, S.; Meng, Y.; Shan, R.; Liang, W.; Zhong, H.; Liao, C.; Yin, X.; Wang, Y. OFDR shape sensor based on a femtosecond-laser-inscribed weak fiber Bragg grating array in a multicore fiber. *Opt. Lett.* **2024**, *49*, 1273–1276. [[CrossRef](#)]
30. Liu, R.; Rozenman, G.G.; Kundu, N.K.; Chandra, D.; De, D. Towards the industrialisation of quantum key distribution in communication networks: A short survey. *IET Quantum Commun.* **2022**, *3*, 151–163. [[CrossRef](#)]
31. Wang, F.; Zhang, L.; Ma, T.; Wang, X.; Yu, K.; Liu, Y. A high-sensitivity sensor based on tapered dispersion compensation fiber for curvature and temperature measurement. *Opt. Commun.* **2021**, *481*, 126534. [[CrossRef](#)]
32. Wu, Y.; Liu, Y.; Zhuang, H.; Cao, J.; Yang, Y.; Zhu, X.; Sun, D.; Shi, Y.; Tao, R. High-sensitivity curvature fiber sensor based on miniature two-path mach-zehnder interferometer. *Micromachines* **2024**, *15*, 963. [[CrossRef](#)]
33. Liu, Z.; Zheng, D.; Madrigal, J.; Villatoro, J.; Antonio-Lopez, J.E.; Schülzgen, A.; Amezcua-Correa, R.; Zou, X.; Pan, W.; Sales, S. Temperature-insensitive curvature sensor based on Bragg gratings written in strongly coupled multicore fiber. *Opt. Lett.* **2021**, *46*, 3933–3936. [[CrossRef](#)]
34. Su, B.; Zhang, F.; Zhong, L.; Qi, B.; Xu, O.; Qin, Y. Temperature compensated curvature sensor with insensitive axial strain based on tapered ring core fiber interferometer. *Opt. Commun.* **2022**, *513*, 128067. [[CrossRef](#)]
35. Wang, S.; Shan, C.; Jiang, J.; Liu, K.; Zhang, X.; Han, Q.; Lei, J.; Xiao, H.; Liu, T. Temperature-insensitive curvature sensor based on anti-resonant reflection guidance and Mach-Zehnder interferometer hybrid mechanism. *Appl. Phys. Express* **2019**, *12*, 106503. [[CrossRef](#)]
36. Zhu, F.; Zhang, Y.; Qu, Y.; Jiang, W.; Su, H.; Guo, Y.; Qi, K. Stress-insensitive vector curvature sensor based on a single fiber Bragg grating. *Opt. Fiber Technol.* **2020**, *54*, 102133. [[CrossRef](#)]
37. Wang, Y.; Richardson, D.; Brambilla, G.; Feng, X.; Petrovich, M.; Ding, M.; Song, Z. Intensity measurement bend sensors based on periodically tapered soft glass fibers. *Opt. Lett.* **2011**, *36*, 558–560. [[CrossRef](#)]
38. Tong, Z.; Luan, P.; Cao, Y.; Zhang, W.; Su, J. Dual-parameter optical fiber sensor based on concatenated down-taper and multimode fiber. *Opt. Commun.* **2016**, *358*, 77–81. [[CrossRef](#)]

Disclaimer/Publisher’s Note: The statements, opinions and data contained in all publications are solely those of the individual author(s) and contributor(s) and not of MDPI and/or the editor(s). MDPI and/or the editor(s) disclaim responsibility for any injury to people or property resulting from any ideas, methods, instructions or products referred to in the content.